

# 中国激光

## 基于非等温流模型与神经网络的光纤拉锥尺寸预测

李力<sup>1</sup>, 郑家容<sup>1,2</sup>, 马修泉<sup>1,3,4\*</sup>

<sup>1</sup>华中科技大学机械科学与工程学院, 湖北 武汉 430074;

<sup>2</sup>广东国志激光技术有限公司, 广东 东莞 523835;

<sup>3</sup>湖北光谷实验室, 湖北 武汉 430074;

<sup>4</sup>数字制造装备与技术国家重点实验室, 湖北 武汉 430074

**摘要** 基于非等温流模型对光纤拉锥过程进行了有限元建模, 实现了多种复杂工况下的光纤拉锥轮廓的计算, 将计算结果与拉锥实验结果进行了对比, 尺寸误差在 6 μm 以内。建立了反向传播(BP)神经网络, 并利用非等温流模拟结果构建训练集进行训练, 实现了对光纤拉锥最终尺寸的快速预测, 预测结果与仿真结果差别最大为 1.7 μm。

**关键词** 光纤光学; 光纤拉锥; 非等温流; 神经网络; 数值模拟

中图分类号 TN253 文献标志码 A

DOI: 10.3788/CJL230502

### 1 引言

光纤拉锥是指对光纤进行加热和拉伸处理进而得到锥形波导结构的工艺<sup>[1]</sup>, 该工艺是制作锥形光纤器件的关键工艺, 在大功率光纤激光<sup>[2-3]</sup>、模分复用<sup>[4-5]</sup>、光纤传感<sup>[6-8]</sup>等领域中具有广泛的应用。光纤锥区显著影响光场的传播状态<sup>[9-10]</sup>, 而光纤锥区与光纤器件的性能直接相关, 因此, 随着各领域对锥形光纤器件性能要求的日益提高, 精确预测锥形光纤尺寸的重要性愈发突出, 既可以避免大量重复、繁琐的拉锥工艺实验, 也有助于促进新的拉锥方法、拉锥设备的出现。

光纤拉锥形状的预测主要有两类较为经典的模型: 基于体积守恒的解析模型与基于流体理论的数值模型。拉锥的体积守恒模型最早由 Birks 等<sup>[1]</sup>提出, 通过对拉锥过程进行一定的假设与简化, 推导出光纤锥区尺寸的解析式。该模型在均匀热区或扫描点热源的工况下具有较好的效果<sup>[11]</sup>, 后续孙伟民等<sup>[12]</sup>将该模型推广到了大热区工况。拉锥的流体模型最早由 Dewynne 等<sup>[13]</sup>提出, 他们将光纤拉制中的理论应用到了光纤拉锥工艺中, 利用玻璃流动的斯托克斯方程得出了一些光纤拉锥成形规律。该模型无法直接得出锥区形状表达式, 而是需要借助有限差分、有限元等算法对流动方程进行求解后, 才可以计算出光纤拉锥尺寸<sup>[14-15]</sup>。

拉锥的解析模型虽然可以直接得出锥区表达式, 但是其模型针对特定工况进行了简化, 适用范围有限。而拉锥的流体模型可以结合成熟数值算法, 通过改变

边界条件实现复杂工况下拉锥尺寸的计算, 虽然也带来了建模流程复杂、计算耗时较长的问题, 但其精度和普适性都较高。本文首先基于有限元法建立光纤拉锥的非等温流模型, 对多种工况下的光纤拉锥过程进行仿真并获得光纤锥区尺寸, 然后建立人工神经网络, 并利用非等温流模型仿真结果作为训练集进行神经网络的训练, 最终实现光纤拉锥尺寸的快速、准确的预测。

### 2 光纤拉锥的非等温流模拟

#### 2.1 光纤拉锥非等温流模型的建立

在有限元软件 Comsol Multiphysics 中建立光纤拉锥的非等温流模型, 利用层流模块、流体传热模块进行非等温流的多物理场耦合, 模型基本方程为

$$\rho \nabla \cdot \mathbf{u} = 0, \quad (1)$$

$$\rho \frac{\partial \mathbf{u}}{\partial t} + \rho (\mathbf{u} \cdot \nabla) \mathbf{u} = \nabla \cdot \left[ -\rho \mathbf{I} + \mu (\nabla \mathbf{u} + (\nabla \mathbf{u})^T) \right], \quad (2)$$

$$\rho C_p \frac{\partial T}{\partial t} + \rho C_p \mathbf{u} \cdot \nabla T + \nabla \cdot \mathbf{q} = 0, \quad (3)$$

式中:  $\rho$  为玻璃密度;  $p$  为压力;  $\mu$  为动力黏度;  $C_p$  为玻璃热容;  $\mathbf{u}$  为流动速度矢量;  $\mathbf{I}$  为单位张量;  $\mathbf{q}$  为热通量矢量;  $T$  为温度。式(1)、(2)分别为质量守恒方程、动量守恒方程, 用于计算光纤拉伸时的流场, 式(3)为能量守恒方程, 主要用于计算光纤受热时的温度分布, 进而获得光纤玻璃的黏度分布。

模型及主要边界条件如图 1 所示: 采用二维轴对称模型( $r$  为径向坐标轴), 以光纤轴线( $z$ )为对称轴建立光纤模型, 矩形区域高度为光纤半径, 宽度为光纤仿真长度; 光纤两端被拉伸, 在光纤左、右边界设置法向

收稿日期: 2023-02-08; 修回日期: 2023-02-23; 录用日期: 2023-03-06; 网络首发日期: 2023-03-13

通信作者: \*xma@hust.edu.cn

速度( $u_z$ )出口边界条件;光纤中段为热源加热区域,在光纤上边界设置广义向内热通量( $q_0$ )边界条件模拟热源对光纤的作用;将光纤区域设置为动网格变形域,并

将上边界设置为外部流体界面。此外,光纤玻璃的拉伸变形也与其自身的物理性质紧密相关,模型中采用的主要物性参数如表 1 所示。

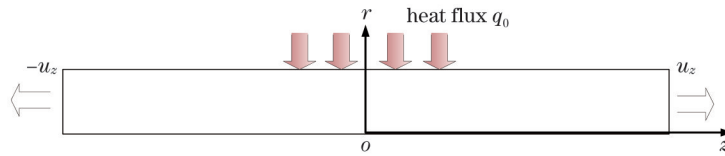


图 1 光纤拉锥非等温流模型及边界条件

Fig. 1 Nonisothermal flow model of fiber tapering and its boundary condition

表 1 仿真所用的玻璃参数

Table 1 Parameters of glass used in simulation

Parameter	Value	Ref.
Density /( $\text{kg}/\text{m}^3$ )	2200	
Surface tension /(N/m)	0.3	[16]
Viscosity /(Pa·s)	$\begin{cases} 3.8 \times 10^{-14} \exp\left(\frac{85640}{T}\right), & T < 1670 \text{ K} \\ 5.8 \times 10^{-8} \exp\left(\frac{61990}{T}\right), & T > 1670 \text{ K} \end{cases}$	[17]
Heat conductivity / [ $\text{W}/(\text{m}\cdot\text{K})$ ]	$\begin{cases} 0.9786 + 1.12 \times 10^{-3}T, & 300 \text{ K} \leqslant T \leqslant 1100 \text{ K} \\ 2.0504 + 1.177 \times 10^{-4}T, & 1100 \text{ K} < T \leqslant 2200 \text{ K} \end{cases}$	[18]
Specific heat capacity / [ $\text{J}/(\text{kg}\cdot\text{K})$ ]	$\begin{cases} 35.936 + 3.3668T - 0.0041T^2 + 2.5803 \times 10^{-6}T^3 - \\ 8.0867 \times 10^{-10}T^4 + 9.9048 \times 10^{-14}T^5, & 273 \text{ K} \leqslant T \leqslant 1973 \text{ K} \\ 1273, & 1973 \text{ K} < T \leqslant 2200 \text{ K} \end{cases}$	[18]

## 2.2 光纤拉锥的模拟

以直径为 360  $\mu\text{m}$  的光纤为研究对象,利用非等温流模型对光纤拉锥进行模拟。将均匀热通量  $q_0=5\times$

$10^5 \text{ W}/\text{m}^2$  施加在光纤轴向  $-2\sim2 \text{ mm}$  区间,拉锥速度为  $1 \text{ mm}/\text{min}$ ,拉锥时间为  $100 \text{ s}$ ,计算结果如图 2 所示。从图 2(a)可以看出,光纤在热通量作用下温度升高到

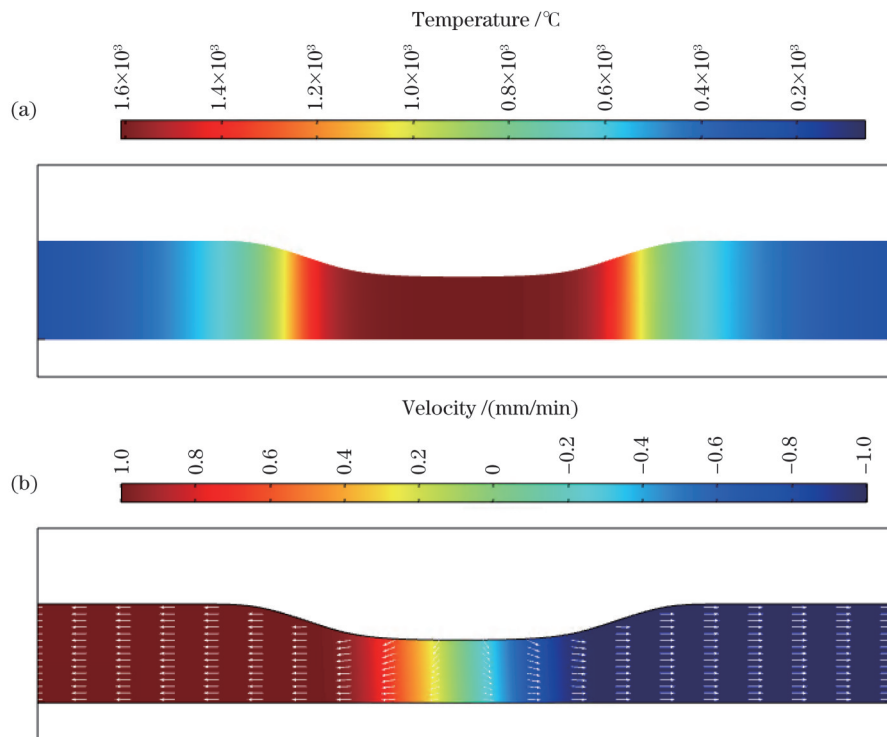


图 2 固定热源下拉锥温度场和速度场分布。(a)温度场;(b)速度场

Fig. 2 Distribution of temperature field and velocity field during tapering under fixed heat source. (a) Temperature field; (b) velocity field

最大(约为 1610 °C),达到光纤玻璃软化点。从图 2(b)可以看出,光纤在拉伸作用下,越靠近中间高温区域玻璃流动速度越小,且该区域边界上玻璃流动速度的径向分量变大,即光纤形变较为剧烈。也可以看出,非等温流模型计算出的锥区轮廓在各处的过渡较为平滑,这是由于模型中温度场是连续变化的,相较于体积守恒模型假设即热区边界温度突变,更加符合实际。

为验证非等温流模型的正确性,进行多种工况下的拉锥仿真,并进行对应的拉锥实验,将二者结果进行对比。仿真采用的主要边界条件为:在光纤轴向上的 -3~3 mm 区间内施加高斯分布热通量  $q_0 = \eta \exp\left\{-\left\{[z - z_c(t)]/\alpha\right\}^2\right\}$ 。其中:系数  $\eta$  控制分布的最大值,此处取  $\eta = 5 \times 10^5$ ;系数  $\alpha$  控制分布的均匀程度,此处取  $\alpha = 4.2 \times 10^{-3}$ ;  $z_c$  为高斯分布中心位置坐标,对于固定热源,  $z_c = 0$ ,对于扫描热源,  $z_c$  为三角波周期函数,控制高斯分布在光纤轴向上的往复移动,三

角波函数的振幅为热源扫描长度的一半,周期为热源扫描长度与热源扫描速度之比的 2 倍。实验采用的设备为氢氧焰拉锥机,拉锥时采用的气体流量为氢气 125 mL/min,氧气 22 mL/min,实验布置如图 3(a)所示。研究的拉锥工况为:光纤拉伸速度为 1 mm/min,热源移动速度为 100 mm/min,拉锥时间为 100 s,热源扫描长度分别为 0、2、4 mm。图 3(b)中点划线、虚线和实线为三种扫描长度下仿真所得的锥区轮廓,三角标志、圆形标志、菱形标志为实验所得的锥区轮廓。可以看出:仿真结果与实验结果吻合度良好,二者尺寸最大差别仅为 6 μm,该差别主要源于仿真参数与实际的区别、实验的重复性误差以及视觉测量误差。同时也注意到,在利用扫描热源进行拉锥的工况下,并没有在光纤中间区域出现尺寸均匀的束腰区域,这是由于热源具有一定长度,在扫描过程中会有一定的重叠效果,且越靠近光纤中间的位置,处于相对高温的时间越长,形变越大。

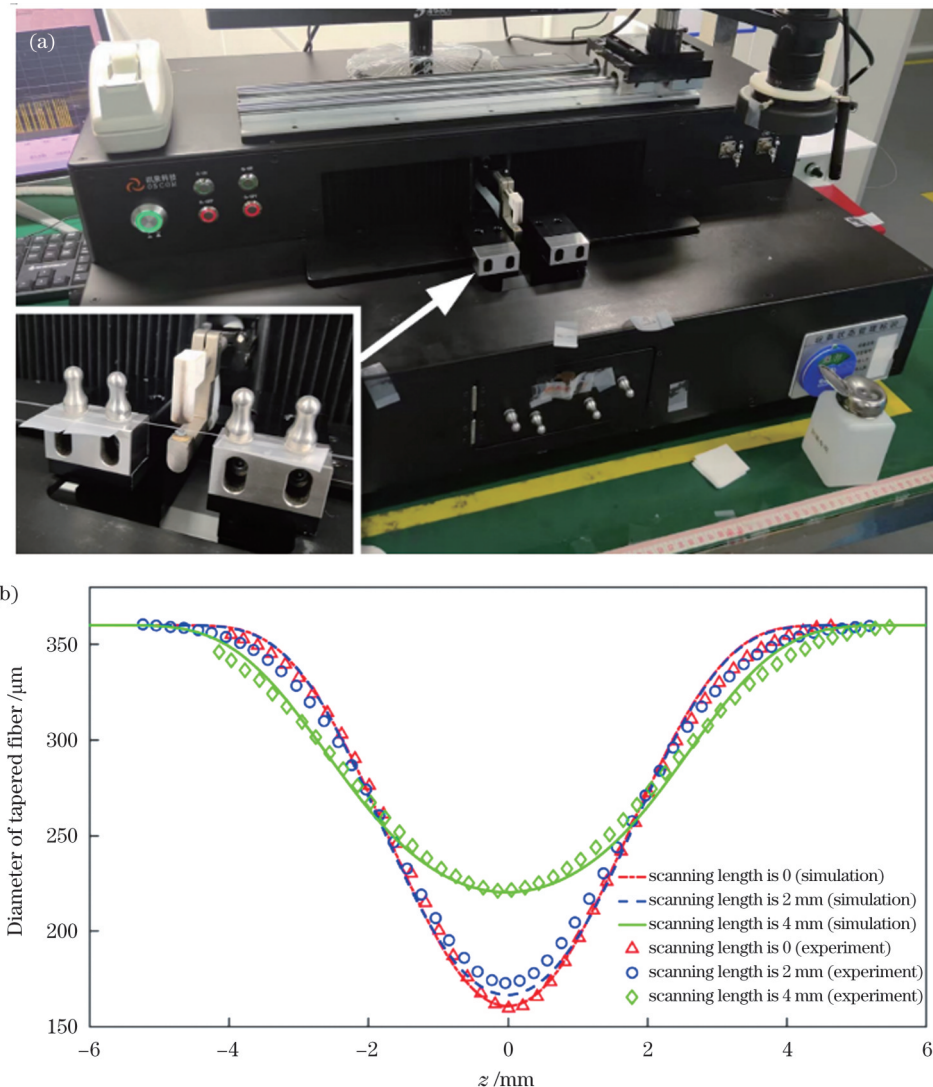


图 3 拉锥轮廓模拟的实验验证。(a)拉锥实验;(b)拉锥轮廓模拟结果与实验结果的对比

Fig. 3 Experimental verification of tapering profile simulation. (a) Tapering experiment; (b) comparison of simulation results and experimental results of tapered profiles

### 3 光纤拉锥尺寸的神经网络预测

非等温流模型的计算结果虽然精度较高,但在工程应用时具有建模环节多、计算耗时的缺点,因此,可以结合机器学习进行锥体尺寸的快速预测,以满足工程应用对便捷性、计算速度的要求。反向传播(BP)神经网络是一种前馈神经网络,包含信号向前传播和误差向后传播的过程,具有很强的对复杂非线性数据映射关系的刻画能力<sup>[19]</sup>,是目前应用最为广泛的机器学

习方法之一<sup>[20-22]</sup>。

在 Matlab 中建立 BP 神经网络,结构包括输入层、隐藏层、输出层,如图 4 所示。输入层神经元包括光纤初始直径、热区长度、热源分布系数( $\alpha$ )和拉锥时间;隐藏层包含两层,神经元个数分别为 5 和 4;输出层为光纤拉锥的最终尺寸。神经网络的学习率为  $1 \times 10^{-4}$ ,最大迭代次数为 1000,训练目标误差为  $1 \times 10^{-10}$ ,网络训练选择 Levenberg-Marquardt 方法。

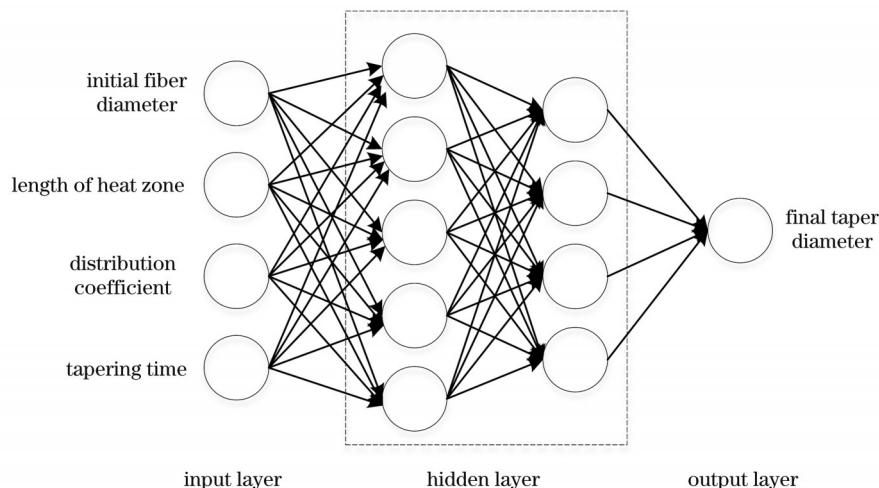


图 4 BP 神经网络的结构  
Fig. 4 Structure of BP neural network

BP 神经网络的训练集采用固定高斯热源的拉锥仿真结果,输入参数包括光纤初始直径(100、200、300、400  $\mu\text{m}$ ),热源长度(4、6、8 mm),热源分布系数  $\alpha$ (0.002、0.003、0.004、0.005),拉锥时间(20、40、60、80、100 s),输出参数为光纤拉锥的最终尺寸,训练集数据共 240 组。训练所得的神经网络均方误差为  $4.03 \times 10^{-5}$ ,精度较高。如图 5 所示,将 10 组 360  $\mu\text{m}$  光纤拉锥仿真结果与神经网络预测结果进行了对比,最大误差为 1.7  $\mu\text{m}$ ,预测效果良好。

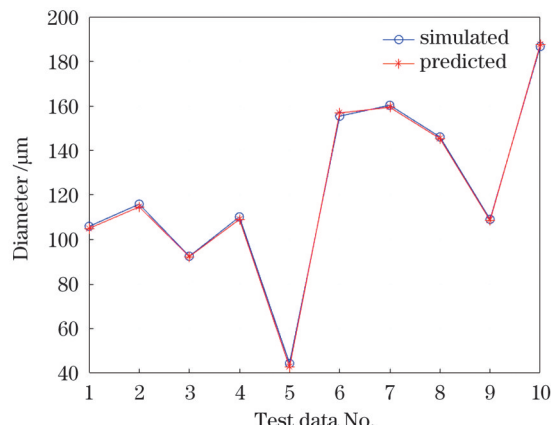


图 5 神经网络预测尺寸与仿真尺寸对比

Fig. 5 Comparison of neural network predicted diameters and simulated diameters

### 4 结 论

采用非等温流模型实现了均匀热源、固定高斯热源以及扫描高斯热源下的光纤拉锥过程模拟,光纤锥区仿真结果与实验结果的差距在 6  $\mu\text{m}$  以内。利用 240 组非等温流模拟结果作为训练集训练了 BP 神经网络,实现了固定高斯热源下的最终拉锥尺寸的预测。神经网络的均方误差为  $4.03 \times 10^{-5}$ ,预测结果与仿真结果的差别最大仅为 1.7  $\mu\text{m}$ 。研究结果为制备锥形光纤器件提供了一种快速、准确的光纤拉锥尺寸预测方法,具有良好的工程应用前景。

### 参 考 文 献

- [1] Birks T A, Li Y W. The shape of fiber tapers[J]. Journal of Lightwave Technology, 1992, 10(4): 432-438.
- [2] Lei C M, Gu Y R, Chen Z L, et al. Incoherent beam combining of fiber lasers by an all-fiber 7×1 signal combiner at a power level of 14 kW[J]. Optics Express, 2018, 26(8): 10421-10427.
- [3] Fu M, Li Z X, Wang Z F, et al. Research on a 4×1 fiber signal combiner with high beam quality at a power level of 12 kW[J]. Optics Express, 2021, 29(17): 26658-26668.
- [4] Yerolatsitis S, Gris-Sánchez I, Birks T A. Adiabatically-tapered fiber mode multiplexers[J]. Optics Express, 2014, 22(1): 608-617.
- [5] Leon-Saval S G, Fontaine N K, Amezcua-Correa R. Photonic lantern as mode multiplexer for multimode optical communications [J]. Optical Fiber Technology, 2017, 35: 46-55.
- [6] Lin H Y, Huang C H, Cheng G L, et al. Tapered optical fiber sensor based on localized surface plasmon resonance[J]. Optics

- Express, 2012, 20(19): 21693-21701.
- [7] Yue C X, Ding H, Ding W, et al. Weakly-coupled multicore optical fiber taper-based high-temperature sensor[J]. Sensors and Actuators A: Physical, 2018, 280: 139-144.
- [8] 徐妍妍, 李俊, 李浩, 等. 基于拉锥七芯光纤的湿度传感器研究[J]. 中国激光, 2021, 48(23): 2306002.
- Xu Y Y, Li J, Li H, et al. Research on humidity sensor based on tapered seven core fiber[J]. Chinese Journal of Lasers, 2021, 48(23): 2306002.
- [9] Love J D, Henry W M, Stewart W J, et al. Tapered single-mode fibres and devices. Part 1: adiabaticity criteria[J]. IEE Proceedings J (Optoelectronics), 1991, 138(5): 343-354.
- [10] Ravets S, Hoffman J E, Kordell P R, et al. Intermodal energy transfer in a tapered optical fiber: optimizing transmission[J]. Journal of the Optical Society of America A, 2013, 30(11): 2361-2371.
- [11] Kenny R P, Birks T A, Oakley K P. Control of optical fibre taper shape[J]. Electronics Letters, 1991, 27(18): 1654-1656.
- [12] 孙伟民, 袁明, 曾宪金, 等. 移动大热区拉锥系统中设定参数对拉锥光纤形状的影响分析[J]. 中国激光, 2011, 38(7): 0705005.
- Sun W M, Yuan M, Zeng X J, et al. Impact analysis of setting parameter of movable large-zone furnace fiber-tapering system to shape of tapered fibers[J]. Chinese Journal of Lasers, 2011, 38(7): 0705005.
- [13] Dewynne J, Ockendon J R, Wilmott P. On a mathematical model for fiber tapering[J]. SIAM Journal on Applied Mathematics, 1989, 49(4): 983-990.
- [14] Xue S C, van Eijkelenborg M A, Barton G W, et al. Theoretical, numerical, and experimental analysis of optical fiber tapering[J]. Journal of Lightwave Technology, 2007, 25(5): 1169-1176.
- [15] Felipe A, Espíndola G, Kalinowski H J, et al. Stepwise fabrication of arbitrary fiber optic tapers[J]. Optics Express, 2012, 20(18): 19893-19904.
- [16] Boyd K, Ebendorff-Heidepriem H, Monro T M, et al. Surface tension and viscosity measurement of optical glasses using a scanning CO<sub>2</sub> laser[J]. Optical Materials Express, 2012, 2(8): 1101-1110.
- [17] Doremus R H. Viscosity of silica[J]. Journal of Applied Physics, 2002, 92(12): 7619-7629.
- [18] Jiang Y, He S B, Liao W, et al. Theoretical and experimental investigations of localized CO<sub>2</sub> laser-fused silica interactions and thermo-mechanical properties of mitigated sites[J]. Journal of Non-Crystalline Solids, 2019, 515: 1-10.
- [19] 焦李成, 杨淑媛, 刘芳, 等. 神经网络七十年: 回顾与展望[J]. 计算机学报, 2016, 39(8): 1697-1716.
- Jiao L C, Yang S Y, Liu F, et al. Seventy years beyond neural networks: retrospect and prospect[J]. Chinese Journal of Computers, 2016, 39(8): 1697-1716.
- [20] 赵黎, 韩中达, 张峰. 基于神经网络的可见光室内立体定位研究[J]. 中国激光, 2021, 48(7): 0706004.
- Zhao L, Han Z D, Zhang F. Research on stereo location in visible light room based on neural network[J]. Chinese Journal of Lasers, 2021, 48(7): 0706004.
- [21] 刘秀航, 黄宇辉, 张艳喜, 等. 基于BP神经网络补偿卡尔曼滤波的激光-MIG复合焊缝熔宽在线检测[J]. 中国激光, 2022, 49(16): 1602011.
- Liu X H, Huang Y H, Zhang Y X, et al. Online weld width detection of laser-MIG hybrid welding based on Kalman filter algorithm compensated by BP neural network[J]. Chinese Journal of Lasers, 2022, 49(16): 1602011.
- [22] 洪哲扬, 薛凌云, 钱依凡. 基于光电热理论和BP神经网络的LED阵列光功率计算方法[J]. 激光与光电子学进展, 2022, 59(5): 0523002.
- Hong Z Y, Xue L Y, Qian Y F. Calculation method of LED array optical power based on photoelectric thermal theory and BP neural network[J]. Laser & Optoelectronics Progress, 2022, 59(5): 0523002.

## Prediction of Optical Fiber Tapering Diameter Based on Nonisothermal Flow Model and Neural Network

Li Li<sup>1</sup>, Zheng Jiarong<sup>1,2</sup>, Ma Xiuquan<sup>1,3,4\*</sup>

<sup>1</sup>School of Mechanical Science and Technology, Huazhong University of Science and Technology, Wuhan 430074, Hubei, China;

<sup>2</sup>GZ Photonics Technology Co., Ltd., Dongguan 523835, Guangdong, China;

<sup>3</sup>Hubei Optics Valley Laboratory, Wuhan 430074, Hubei, China;

<sup>4</sup>State Key Laboratory of Digital Manufacturing Equipment and Technology, Wuhan 430074, Hubei, China

### Abstract

**Objective** Optical fiber tapering is a key process in the fabrication of optical fiber devices such as fiber combiners, fiber sensors, and fiber multiplexers. The tapered section has a significant influence on the light propagation state and directly relates to the performance of the fiber devices. Consequently, the precise prediction of the diameters of tapered optical fibers is increasingly important for the design and fabrication of high-performance optical devices. A straightforward and convenient analytical model based on volume conservation during the optical fiber deformation process can be used to obtain the expressions for the tapered optical fibers. However, this model only focuses on the tapering process under an ideal uniform heat source and scanning point heat source. A fluid dynamics model is an alternative method for studying the tapering process of optical fibers. With the help of numerical methods such as finite element method and finite difference method, the fluid dynamics model can also be used to obtain the diameters of the tapered optical fibers. Because more practical boundary conditions can be applied, the fluid dynamics model is applicable to the tapering process under complicated conditions, such as scanning nonuniform heat sources. In this study, a nonisothermal flow model is built using the finite element method to study the tapering process of optical fibers. With the tapering diameters obtained from the nonisothermal flow model, a back propagation (BP) neural network is then built and trained to achieve fast prediction of the tapering diameter for engineering applications.

**Methods** First, a nonisothermal flow model of optical fiber tapering is implemented in the finite element software COMSOL Multiphysics. A two-dimensional axisymmetric model of optical fiber is built, normal outflow velocity is applied to both ends of the optical fiber, and general inward heat flux and free surface conditions are applied to the surface of the optical fiber (Fig. 1). With this numerical model, the tapering of optical fibers under different conditions can be simulated. Second, tapering experiments are conducted using tapering equipment with an oxyhydrogen flame (Fig. 3(a)), and the tapered optical fibers are then scanned to obtain the diameters. The comparison of the simulation and experimental results verifies the validity of the nonisothermal flow model. Third, a BP neural network including one input layer, two hidden layers, and one output layer is built in Matlab (Fig. 4). The input of the network includes the initial fiber diameter, length of the heat zone, distribution coefficient of the heat source, and tapering time, and the output of the network is the final taper diameter. The training dataset for the network is generated using the simulation results of the tapering diameters under a fixed Gaussian heat source. Specifically, the training dataset includes 240 simulations with initial input diameters of 100, 200, 300, and 400  $\mu\text{m}$ , heat zone lengths of 4, 6, and 8 mm, heat source distribution coefficients of 0.002, 0.003, 0.004, and 0.005, and tapering time of 20, 40, 60, 80, and 100 s.

**Results and Discussions** The diameter differences between tapered profiles calculated using the nonisothermal flow model and those measured in the tapering experiments are within 6  $\mu\text{m}$ , which verifies the accuracy of this numerical model (Fig. 3(b)). The simulation also successfully predicts the absence of a waist in the tapered profile, which is due to the nonuniform temperature distribution in the heat zone and the overlap effect of the heat source during scanning. The BP neural network predicts the tapering diameter of 360  $\mu\text{m}$  fiber, and the difference between the predicted and simulated results is within 1.7  $\mu\text{m}$  (Fig. 5).

**Conclusions** In this study, the tapering processes under a uniform heat source, fixed Gaussian heat source, and scanning Gaussian heat source are successfully simulated using a nonisothermal flow model. The simulation results for the tapered profiles are in good agreement with the tapering experimental results, and the differences are within 6  $\mu\text{m}$ . A BP neural network is built and trained with the dataset obtained from the nonisothermal flow simulations. Fast prediction of the final tapering diameters of optical fibers is achieved, and the difference between the predicted and simulated results is within 1.7  $\mu\text{m}$ .

**Key words** fiber optics; fiber tapering; nonisothermal flow; neural network; numerical simulation